Journal of Magnetic Resonance **143,** 136–143 (2000)
doi:10.1006/jmre.1999.1971, available online at http://www.idealibrary.com on IDEAL®

Spin Dynamics of Polarization Inversion Spin Exchange at the Magic Angle in Multiple Spin Systems

Zhehong Gan

Center of Interdisciplinary Magnetic Resonance, National High Magnetic Field Laboratory, 1800 East Paul Dirac Drive, Tallahassee, Florida 32310

Received July 13, 1999; revised October 29, 1999

Polarization inversion spin exchange at the magic angle (PISEMA) [*J. Magn. Reson. A* 109, 270 (1994)] is an important experiment in NMR structural characterization of membrane proteins in oriented lipid bilayers. This paper presents a theoretical and experimental study of the spin dynamics in PISEMA to investigate the line-narrowing mechanism. The study focuses on the effect of neighboring protons on the spin exchange of a strongly coupled spin pair. The spin exchange is solved analytically for simple spin systems and is numerically simulated for many-spin systems. The results show that the dipolar couplings from the neighboring protons of a strongly coupled spin pair perturb the spin exchange only in the second order, therefore it has little contribution to the linewidth of PISEMA spectra in comparison to the separated-local-field spectra. The effects from proton resonance offset and the mismatch of the Hartmann–Hahn condition are also discussed along with experimental results using model single-crystal samples.

Key Words: **spin exchange; PISEMA; line narrowing; multiple spin effect.**

1. INTRODUCTION

Nuclear spin dipolar coupling $D_{ij} = (\mu_0\gamma_i\gamma_j h/8\pi^2 r_{ij}^3) P_2(\cos\theta_{ij})$ depends not only on the internuclear distance, r_{ij}, but also on the orientation of the internuclear vector to the applied magnetic field, θ_{ij}. For polycrystalline samples, the superposition of the dipolar coupling over θ_{ij} yields the well-known Pake pattern (*1*) from which the internuclear distance can be measured. For oriented samples, the dipolar coupling of a spin pair with known bond length, e.g., ^{13}C–^{1}H and ^{15}N–^{1}H, yields directly the orientation of the bond vector to the magnetic field. For the measurement of the heteronuclear coupling, proton homonuclear decoupling is required as the spin pair usually strongly interacts with a proton coupling network (*2*). Furthermore, the separated-local-field (SLF) experiment can separate heteronuclear dipolar coupling by chemical shift in a two-dimensional (2D) spectrum and the dipolar couplings of numerous spin pairs can be measured from a single 2D experiment (*2–4*).

Heteronuclear dipolar coupling can also be measured through the transient oscillation of spin exchange induced by the flip-flop terms, $H_{Si} = D_{Si}(S_+I_-^i + S_-I_+^i)/2$, of the dipolar Hamiltonian (*3, 5*). The polarization inversion spin exchange at the magic angle (PISEMA) experiment (*6*) combines the spin exchange scheme and the frequency-switched Lee–Goldberg (FSLG) proton homonuclear decoupling sequence (*7, 8*) and it achieves an order of magnitude in line narrowing over the SLF experiment. The line narrowing dramatically improves the spectral resolution required to resolve the large number of chemical sites in complex systems and the PISEMA experiment has been successfully applied in the structure determination of membrane proteins in oriented lipid bilayers (*9–11*).

Several mechanisms contribute to the line narrowing in the PISEMA experiment. It has been attributed that the decay of spin exchange is governed by the spin–lattice relaxation time in the rotating frame, $T_{1\rho}$, which is usually much longer than T_2 (*6*). The study here focuses on the dipolar couplings from the neighboring protons and their contribution to the linewidth in PISEMA and SLF spectra. In the SLF experiment, each of these protons adds a splitting to the dipolar spectrum and the superposition of various weak couplings from numerous surrounding protons effectively broadens the spectral lines. In the PISEMA experiment, the linebroadening effect from neighboring protons is not straightforward. In the flip-flop form, the dipolar couplings from various protons do not commute $[H_{Si}, H_{Sj}] \neq 0$ and the spin exchange cannot be generally solved for multiple spin systems. In the following, the spin exchange in simple XH, XH$_2$, XH$_3$ (X = ^{13}C or ^{15}N) spin systems is treated analytically and computer simulations are used to study the spin exchange in many-spin systems. The comparison between the resulting PISEMA spectra and the corresponding SLF spectra reveals drastic differences in line broadening between the two experiments. The effects from the proton resonance offset and the mismatch of the Hartman–Hahn condition are also studied along with experimental results using model single-crystal samples.

1090-7807/00 $35.00

2. THEORY

2.1. Spin Hamiltonian

In a NMR experiment, the spin Hamiltonian generally consists of the interaction with the applied radiofrequency (RF) magnetic field and the internal Hamiltonian of the spin systems,

$$H = H_{\mathrm{RF}} + H_{\mathrm{int}}. \qquad [1]$$

For an S spin interacting with a group of proton (I) spins, the internal Hamiltonian includes the chemical shift, the heteronuclear dipolar coupling, and the homonuclear dipolar coupling among the I spins,

$$\begin{aligned} H_{\mathrm{int}} &= H_{\mathrm{CS}} + H_{SI} + H_{II}, \\ H_{\mathrm{CS}} &= \Delta\omega_S S_z + \sum_i \Delta\omega_I^i I_z^i, \\ H_{SI} &= \sum_i D_{Si} 2 S_z I_z^i, \\ H_{II} &= \sum_{i<j} D_{ij}[2I_z^i I_z^j - (I_+^i I_-^j + I_-^i I_+^j)], \end{aligned} \qquad [2]$$

where $D_{ij} = (\mu_0 \gamma_i \gamma_j h/8\pi^2 r_{ij}^3) P_2(\cos\theta_{ij})$ are the dipolar coupling frequencies. The RF Hamiltonian can be generally written as

$$\begin{aligned} H_{\mathrm{RF}} = {} & \omega_{1S}(\cos\varphi_S S_x + \sin\varphi_S S_y) \\ & + \sum_i \omega_{1I}(\cos\varphi_I I_x^i + \sin\varphi_I I_y^i), \end{aligned} \qquad [3]$$

where $\omega_{1S} = -\gamma_S B_{1S}$ and $\omega_{1I} = -\gamma_I B_{1I}$ represent the applied RF irradiation with phase φ_S and φ_I to the S and I spins, respectively.

The PISEMA pulse sequence shown in Fig. 1 combines the frequency-switched Lee–Goldberg sequence (*7, 8*) with the Hartmann–Hahn cross polarization (*12, 13*) for measuring the spin exchange under proton homonuclear decoupling. During the FSLG sequence, the ^{1}H effective field is tilted by the frequency offset. It is convenient to rotate the reference frame through substituting the spin operators $I_x^i \rightarrow \cos\theta_M I_x^i + \sin\theta_M I_z^i$, $I_y^i \rightarrow I_y^i$, $I_z^i \rightarrow \cos\theta_M I_z^i - \sin\theta_M I_x^i$ such that the effective field is along the z axis. In this tilted frame, the RF Hamiltonian becomes

$$H_{\mathrm{RF}} = s(t)(\omega_{1S} S_z + \sum_i \omega_I^{\mathrm{eff}} I_z^i), \qquad [4]$$

where $\omega_I^{\mathrm{eff}} = -\gamma_I B_I^{\mathrm{eff}}$. The sign, $s(t)$, denotes the inversion of

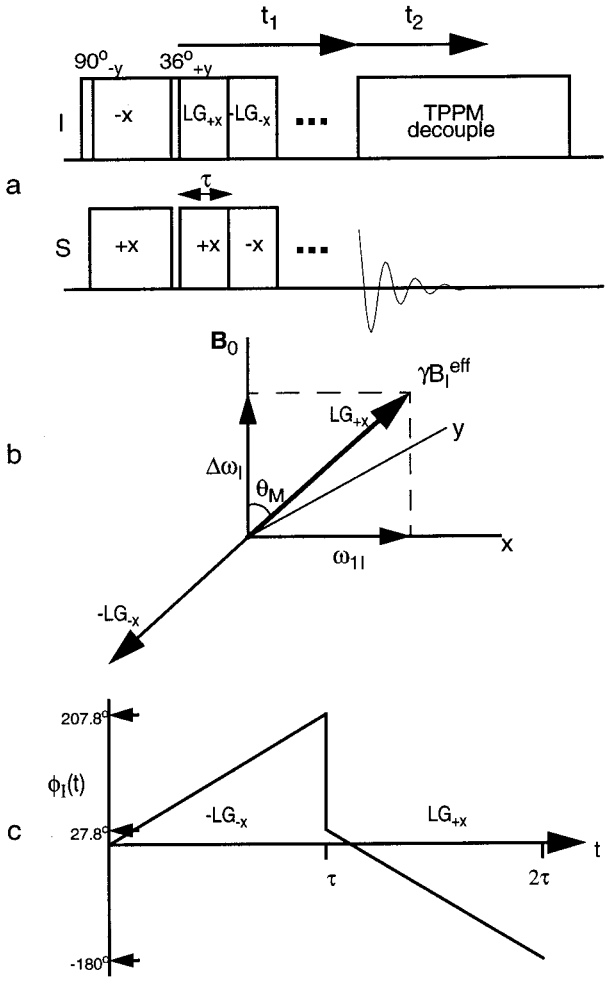

FIG. 1. (a) PISEMA pulse sequence. (b) ^{1}H effective field during FSLG homonuclear decoupling sequence. (c) Phase ramp which can be used to generate the FSLG sequence.

the effective fields of the I and S spins by the frequency and phase shift. Under strong RF irradiation, the internal spin Hamiltonian is truncated by the RF Hamiltonian and only the terms which commute with the RF Hamiltonian remain in the average Hamiltonian. Thus, the off-resonant ^{1}H RF irradiation scales the proton chemical shift by $\cos\theta_M$,

$$H_{\mathrm{CS}} = \sum_i \cos\theta_M \Delta\omega_I^i I_z^i, \qquad [5]$$

and the homonuclear dipolar interaction by $P_2(\cos\theta_M)$,

$$H_{II} = \sum_{i<j} P_2(\cos\theta_M) D_{ij}[2I_z^i I_z^j - (I_+^i I_-^j + I_-^i I_+^j)]. \qquad [6]$$

The homonuclear dipolar coupling becomes zero when the I spin effective field is at the magic angle, $\tan\theta_M = \omega_{1I}/\Delta\omega_I =$

$\sqrt{2}$. The repeated inversion of the ^{1}H effective field with an interval $\tau = 2\pi/\sqrt{\omega_{1I}^2 + \Delta\omega_I^2}$ further suppresses the high-order terms in the average Hamiltonian of the FSLG pulse sequence (*8*). Figure 1 also shows the phase ramp which generates the FSLG decoupling sequence. A frequency shift is equivalent to a time-dependent RF phase, $\varphi_I(t) = \int_0^t \Delta\omega_I(t')dt'$.

The heteronuclear dipolar interaction remains when the amplitudes of two effective fields are near the Hartmann–Hahn condition $\omega_{1S} = \omega_I^{\text{eff}}$. The dipolar Hamiltonian takes the flip-flop terms and it is scaled by $\sin\theta_M$,

$$H_{SI} = \sum_i \sin\theta_M D_{Si} \frac{(S_+ I_-^i + S_- I_+^i)}{2}. \qquad [7]$$

Small mismatch of the Hartmann–Hahn condition can be taken into account by a mismatch term in the RF Hamiltonian. The phase and frequency switching alters the sign, $s(t)$, and it averages the mismatch term after a complete FSLG cycle. In Fig. 1a, a 90°–θ_M pulse is applied immediately before the evolution period in the PISEMA pulse sequence. This pulse is used to maximize the difference of polarization between the *S* and the *I* spins for spin exchange,

$$\sigma(0) \propto S_z - F_z. \qquad [8]$$

In the SLF experiment, the heteronuclear dipolar coupling takes the $2S_zI_z^i$ term and it is scaled by cos θ_M with the FSLG sequence used for homonuclear decoupling,

$$H_{SI}^{\text{SLF}} = \sum_i \cos\theta_M D_{Si} 2S_z I_z^i. \qquad [9]$$

2.2. Spin Exchange in a Two-Spin System

First we consider the spin exchange in an isolated two-spin *IS* system. The evolution under the heteronuclear dipolar coupling $H_{SI} = \sin\theta_M D_{SI}\ (S_+I_- + S_-I_+)/2$ can be obtained analytically,

$$\sigma(t) = e^{-iH_{SI}t}\sigma(0)e^{iH_{SI}t} \propto (S_z - I_z)\cos(\sin\theta_M D_{SI} t) + i(S_+I_- - S_-I_+)\sin(\sin\theta_M D_{SI} t). \qquad [10]$$

Thus the dipolar coupling converts the difference in polarization into two-spin order $S_xI_y - S_yI_x$. The spin exchange leads to the signal

$$s(t) = \text{Tr}[S_z\sigma(t)] = s(0)\cos(\sin\theta_M D_{SI} t), \qquad [11]$$

which yields a doublet separated by $2\sin\theta_M D_{SI}$ in the frequency domain.

The treatment of the two-spin system can be extended to the Liouville space such that the relaxation effect from the lattice can be considered. The base operators, $B_1 = (S_z - I_z)/2$, $B_2 = (S_+I_- + S_-I_+)/2$, and $B_3 = -i(S_+I_- - S_-I_+)/2$, are sufficient to describe the evolution in the Liouville space under the Hamiltonian, $H = H_{SI} + H_{CS}$,

$$\frac{d}{dt} a_i(t) = \sum_i W_{ij} a_j(t), \qquad [12]$$

$$W_{ij} = \frac{\text{Tr}\{iH[B_i, B_j] + B_i\hat{\Gamma}B_j\}}{\text{Tr}\{B_i^2\}} = \begin{bmatrix} -R_1 & 0 & \sin\theta_M D_{SI} \\ 0 & -R_2 & -\Delta\omega_I \cos\theta_M \\ -\sin\theta_M D_{SI} & \Delta\omega_I \cos\theta_M & -R_3 \end{bmatrix}. \qquad [13]$$

In Eqs. [12] and [13], $a_i(t)$ are the expansion coefficients of the density operator and $\hat{\Gamma}$ is the relaxation superoperator (*14*). Along the diagonal of the rate matrix, R_1 is the rate constant for the decay of spin polarization, $S_z - I_z$, and $R_2 = R_3$ is the rate constant for the decay of two-spin coherences. A simple solution can be obtained when $R_1 \approx R_2 = R$,

$$s(t) = s(0)\left[\sin^2\xi + \cos^2\xi \cos\left(\frac{\sin\theta_M D_{SI}}{\cos\xi} t\right)\right] e^{-Rt}, \qquad [14]$$

where $\tan\xi = \Delta\omega_I\cos\theta_M/D_{SI}\sin\theta_M$. The proton resonance offset introduces a constant component, $\sin^2\xi$, in the time domain signal which corresponds to a central peak in the dipolar spectrum. The offset also changes the oscillation frequency to $\sqrt{(\sin\theta_M D_{SI})^2 + (\Delta\omega_I\cos\theta_M)^2}$ and it makes the splitting larger. The transient oscillation of spin exchange is damped by *R*. In addition to the spin–lattice relaxation in the rotating frame, $T_{1\rho}$, of the *S* spin, the spin diffusion among the protons also contributes to the rate constants. Depending on the homonuclear decoupling efficiency, proton spin-diffusion caused by the residual homonuclear coupling can become dominant in the contribution to the damping of spin exchange.

2.3. Spin Exchange in a Many-Spin System

Spin exchange in two kinds of many-spin systems will be treated analytically: an SI_2 three-spin system and an *S* spin coupled to *N* magnetically equivalent *I* spins. For the SI_2 three-spin system, H_{SI} is a sum of the heteronuclear dipolar couplings from the two protons,

$$H_{SI} = \sin\theta_M \left[S_+ \frac{(D_{S1}I_-^1 + D_{S2}I_-^2)}{2} + S_- \frac{(D_{S1}I_+^1 + D_{S2}I_+^2)}{2} \right]. \qquad [15]$$

For the matrix presentation of the Hamiltonian, the proton spin states, $\sin\alpha|+\ -\rangle - \cos\alpha|-\ +\rangle$, $|+\ +\rangle$, $\sin\alpha|+\ -\rangle + \cos\alpha|-\ +\rangle$, and $|-\ -\rangle$ with $\tan\alpha = D_{S2}/D_{S1}$ are chosen as the base kets. The I spin operators in H_{SI} can then be explicitly written as

$$\frac{D_{S1}I_-^1 + D_{S2}I_-^2}{\sqrt{D_{S1}^2 + D_{S2}^2}} = \begin{bmatrix} 0 & 0 & 0 & 0 \\ \bar{0} & 0 & \bar{1} & \bar{0} \\ 0 & 0 & 0 & 1 \\ 0 & 0 & 0 & 0 \end{bmatrix},$$

$$\frac{D_{S1}I_+^1 + D_{S2}I_+^2}{\sqrt{D_{S1}^2 + D_{S2}^2}} = \begin{bmatrix} 0 & 0 & 0 & 0 \\ \bar{0} & 0 & \bar{0} & \bar{0} \\ 0 & 1 & 0 & 0 \\ 0 & 0 & 1 & 0 \end{bmatrix}. \qquad [16]$$

The Hamiltonian contains only the elements within the three I spin states: $|+\ +\rangle$, $\sin\alpha|+\ -\rangle + \cos\alpha|-\ +\rangle$, $|-\ -\rangle$. The corresponding 3×3 subspace can be expressed by a spin operator, $F = 1$. Therefore, the dipolar Hamiltonian can be rewritten as

$$H_{SI} = \sin\theta_M \sqrt{(D_{S1}^2 + D_{S2}^2)/2}\ \frac{(S_+F_- + S_-F_+)}{2}. \qquad [17]$$

In the case of an S spin coupled to N proton spins with an equal coupling frequency, the heteronuclear dipolar coupling Hamiltonian can also be expressed in the form of Eq. [17] with F up to N.

The spin exchange under the Hamiltonian, $H_{SI} = D(S_+F_- + S_-F_+)$, can be obtained analytically for arbitrary F. The Hamiltonian is diagonalized in the following eigenstates with their corresponding eigenvalues,

$$|\alpha f\rangle \cdots \frac{|\alpha m\rangle \pm |\beta m-1\rangle}{\sqrt{2}} \cdots |\beta -f\rangle,$$
$$0 \cdots \pm D\sqrt{(f+m)(f-m+1)} \cdots 0, \qquad [18]$$

where $|\alpha\rangle$ and $|\beta\rangle$ represent the two S spin states and m runs from $-f+1$ to f for the F spin. The spin operators which are relevant to the spin exchange have matrix elements exclusively within the pairs of eigenstates, $(|\alpha m\rangle \pm |\beta\ m-1\rangle)/\sqrt{2}$,

$$(S_z)_m = \begin{bmatrix} 0 & \frac{1}{2} \\ \frac{1}{2} & 0 \end{bmatrix},\ (F_z)_m = \begin{bmatrix} m-\frac{1}{2} & -\frac{1}{2} \\ -\frac{1}{2} & m-\frac{1}{2} \end{bmatrix},$$

$$(H_{SI})_m = D\sqrt{(f+m)(f-m+1)} \begin{bmatrix} 1 & 0 \\ 0 & -1 \end{bmatrix}. \qquad [19]$$

Therefore, the evolution of the S spin magnetization has the following oscillating components:

$$\sum_{m=-f+1}^{f} \mathrm{Tr}\{(S_z)_m e^{-i(H_{SI})_m t}[(S_z)_m - (F_z)_m]e^{i(H_{SI})_m t}\}$$
$$= \sum_{m=-f+1}^{f} 2\cos(D\sqrt{(f+m)(f-m+1)}t). \qquad [20]$$

In the case of the SI_2 three-spin system, $F = 1$, the two oscillating components, $m = 0, 1$, have the same frequency,

$$s(t) = s(0)\cos[(\sin\theta_M \sqrt{D_{S1}^2 + D_{S2}^2})t]. \qquad [21]$$

A Fourier transformation of the signal yields a doublet separated by $2\sin\theta_M \sqrt{D_{S1}^2 + D_{S2}^2}$. For a rapid rotating methyl group, the heteronuclear dipolar Hamiltonian can be expressed in a subspace of an S spin coupled to an $F = \frac{3}{2}$ spin and two subspaces of an S spin coupled to an $F = \frac{1}{2}$ spin. From Eq. [20], the spin exchange in the $F = \frac{3}{2}$ space has two frequencies, $\sqrt{3}\sin\theta_M D$ $(m = \frac{3}{2},\ -\frac{1}{2})$ and $2\sin\theta_M D$ $(m = \frac{1}{2})$, with an amplitude ratio of 2:1. In the $F = \frac{1}{2}$ subspaces, the spin exchange has one frequency, $\sin\theta_M D$. Therefore, the PISEMA spectra of a methyl group shows six peaks in Fig. 2.

3. RESULTS AND DISCUSSION

Figure 2 shows the comparison between PISEMA and SLF spectra of SI, SI_2, and SI_3 spin systems. For an isolated spin pair, the two experiments yield similar spectra differing only by the scaling factor which favors PISEMA by $\tan\theta_M = \sqrt{2}$. For an SI_2 group, the SLF spectrum shows four peaks corresponding to the four spin states of the two protons; however, the PISEMA spectrum remains as a doublet with splitting, $2\sin\theta_M\sqrt{D_{S1}^2 + D_{S2}^2}$. The spectra are also different between the two experiments for a methyl group. The splitting in the SI_2 case can be used to estimate the effect from one neighboring proton to the PISEMA spectrum of a strongly coupled spin pair. The neighboring proton does not cause any additional splitting and, when $D_{S1} \gg D_{S2}$, it merely perturbs the splitting by $(D_{S2}^2/2D_{S1})\sin\theta_M$, which is a second-order effect.

Figure 3 shows the simulations of spin systems with up to five protons and it further demonstrates the difference in line broadening from neighboring protons between the PISEMA and the SLF experiments. In the simulations, $D_{S1} = 10$ kHz represents a typical strongly coupled spin pair and various weak dipolar couplings are used to simulate the effect from the neighboring protons. The weak dipolar couplings cause multiplets in the SLF spectra and they broaden the dipolar spectrum of the $D_{S1} = 10\ kHz$ spin pair. In contrast, the PISEMA spectra are merely perturbed by the various weak couplings. The linewidth of the doublet remains narrow and spectral expansion is required to see the multiple spin effect in Fig. 3. The center frequency of the multiplet is slightly shifted by the

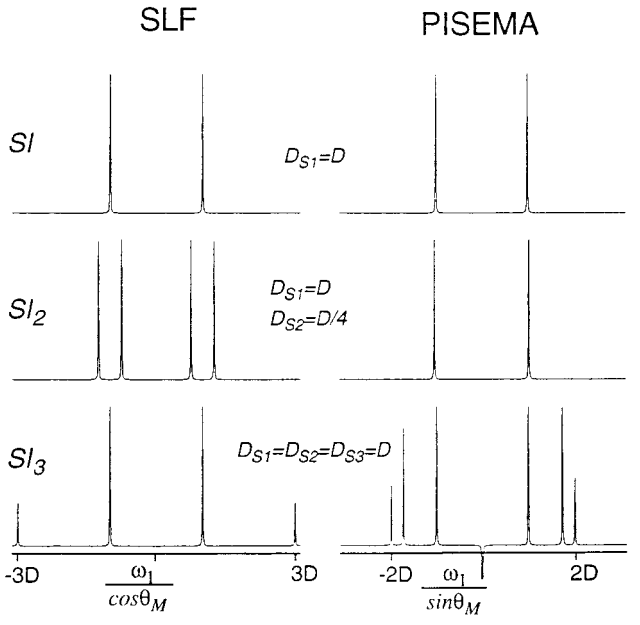

FIG. 2. Simulations of SLF (left) and PISEMA (right) spectra of *SI*, SI_2, and SI_3 spin systems. The frequency axes are scaled by $\cos\theta_M$ and $\sin\theta_M$ in the SLF and PISEMA spectra, respectively, because of the FSLG ^{1}H homonuclear decoupling.

weak couplings. The shift, estimated at about $\Sigma_{i>1}$ $(D_{Si}^2/2D_{S1})\sin\theta_M$, makes the apparent splitting slightly larger, and it could have an effect on the measurement of dipolar splitting. The addition of weakly coupled protons also causes small peaks near the zero frequency in the PISEMA spectra.

The line-narrowing mechanism in PISEMA can be explained by the truncation of the weak dipolar couplings from the neighboring protons by the much larger dipolar Hamiltonian of the strongly coupled spin pair. In the SLF experiment, the heteronuclear dipolar coupling Hamiltonians from various protons commute with each other and no truncation takes place. Each addition of a proton causes a splitting with its dipolar coupling frequency. In the PISEMA experiment, the flip-flop terms of the dipolar Hamiltonian do not commute with the dominant term from the strongly coupled spin pair. Thus, the weak coupling terms from the neighboring protons are effectively truncated resulting in much narrower lines in comparison with that in the SLF experiment.

Figure 4 shows the spectrum of a glycine single-crystal sample to demonstrate the PISEMA experiment of a CH_2 group. The unit cell of the single crystal has four molecules which are related in pair by inversion symmetry (*15*), therefore there are two magnetically inequivalent methylene and carboxyl sites in the single-crystal sample. The spectrum in Fig. 4

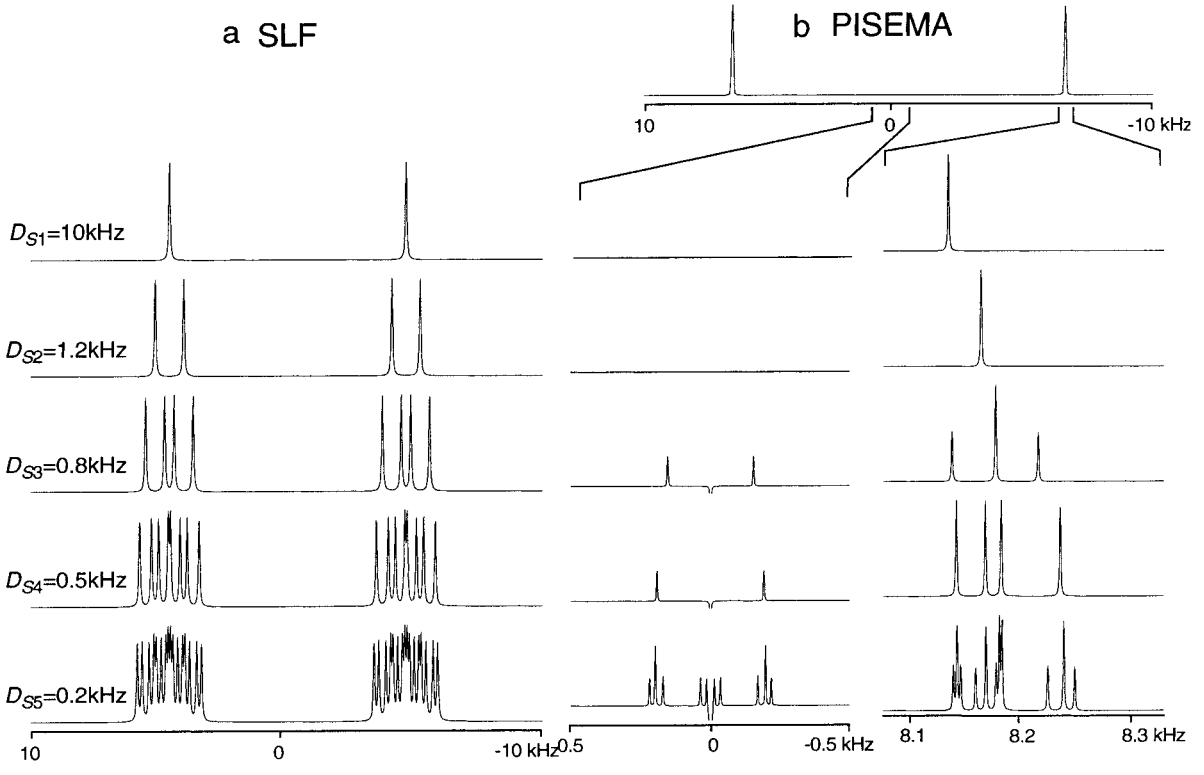

FIG. 3. Comparison of (a) SLF and (b) PISEMA spectra simulated, from top to bottom, for 2-, 3-, 4-, 5-, and 6-spin systems. The spectra were calculated numerically using the Hamiltonian including only the heteronuclear dipolar coupling, $H_{\mathrm{SLF}} = \Sigma_i \cos\theta_M D_{Si} 2S_z I_z^i$ and $H_{\mathrm{PISEMA}} = \Sigma_i \sin\theta_M D_{Si} (S_+ I_-^i + S_- I_+^i)/2$ with the coupling frequencies D_{Si} listed in the figure. In the PISEMA spectra, the expansions near the main doublet and the central region are plotted.

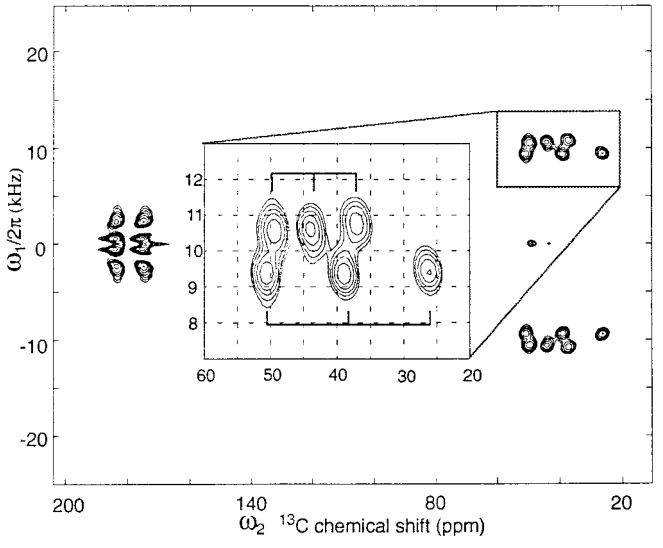

FIG. 4. 2D PISEMA spectrum of a glycine single crystal at an arbitrary crystal orientation. The inset shows the spectral region of the methylene groups. The spectrum was acquired at room temperature on a 300-MHz Bruker Avance DMX spectrometer equipped with a 4-mm MAS probe operated in static mode. The ^{1}H RF field, $\gamma B_{1I}/2\pi$, was set to 100 kHz during a 1-ms cross polarization and the t_2 period and was lowered to 82 kHz during the t_1 period. The ^{13}C RF field, $\gamma B_{1S}/2\pi$, was 100 kHz, satisfying the Hartmann–Hahn condition during both the cross polarization and the t_1 period for spin exchange. For better timing control of the phase and frequency shift, the FSLG sequence was implemented by the RF phase ramp shown in Fig. 1c using the waveform generator of the spectrometer. The generated frequency shift was determined by the slope of the phase ramp, $\Delta\omega_I = (\pm 2\pi\cos\theta_M)/\tau$. A total of 64 t_1 increments were acquired for the 2D experiment with 128 scans for each t_1 increment and a 1-s delay between scans. The single crystal, about $2 \times 2 \times 5$ mm in size, was grown from slow evaporation of an aqueous solution.

shows doublets along the ω_1 dimension for CH_2 groups and it is in agreement with the results from the theory and the simulations. Along the ω_2 dimension, the methylene peaks are split into triplets due to the dipolar coupling to the nearby ^{14}N spin. The spacings within a triplet are slightly different due to the large ^{14}N quadrupolar interaction (*16–25*). The ^{13}C–^{14}N dipolar coupling frequency, however, can be measured from the splitting between the two outer peaks, because the second-order quadrupolar effects are the same for the $m = +1, -1$ ^{14}N spin states.

The spectra of methyl-α-D-glucopyranoside in Fig. 5 demonstrate the effect of line narrowing to the spectral resolution of a system with many sites. The four inequivalent molecules per unit cell cause 28 lines for the single-crystal sample. Many peaks that are overlapped in the SLF spectrum become resolved in the PISEMA spectrum. In the PISEMA spectrum, the peaks with smaller splittings show more complicated lineshape than the peaks with larger splittings. This difference comes from the fact that the truncation becomes less effective when the dipolar couplings from neighboring protons are comparable to that of the ^{13}C–^{1}H spin pair.

The match of the Hartmann–Hahn condition is critical for spin exchange. In the PISEMA experiment, the effective fields are repeatedly inverted and the alternation of the sign, $s(t)$, in the RF Hamiltonian averages the mismatch of the two effective fields. PISEMA spectra with a mismatch of RF fields up to 12

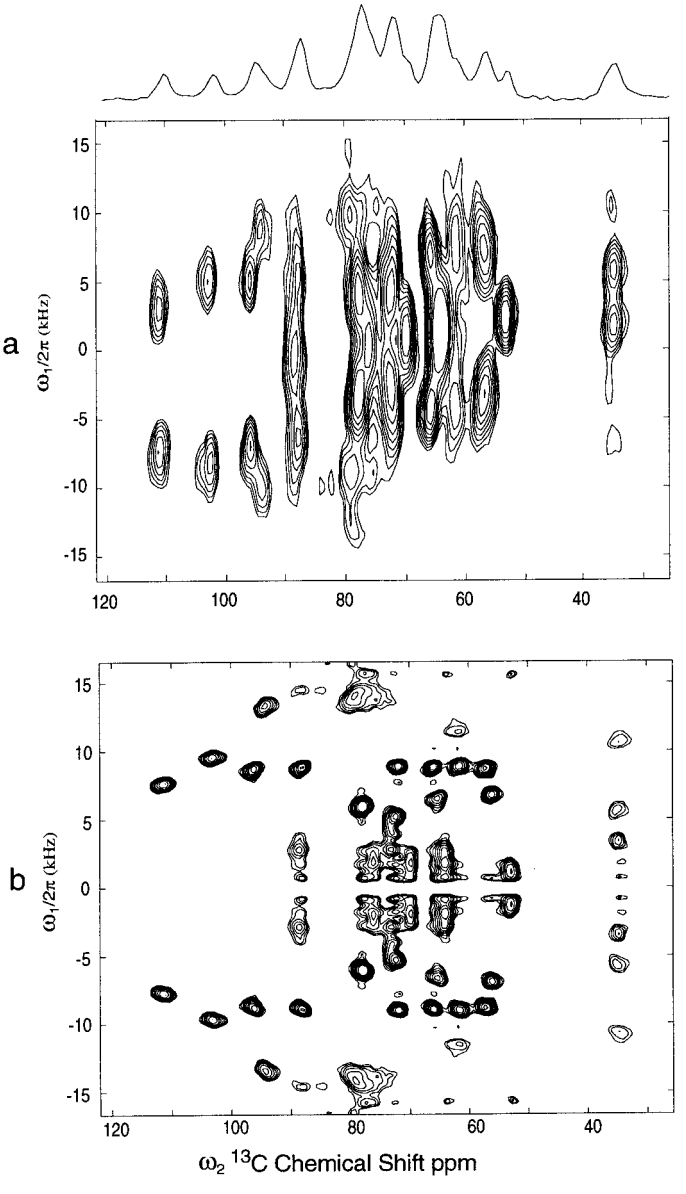

FIG. 5. (a) SLF and (b) PISEMA spectra of a methyl-α-D-glucopyranoside single crystal at an arbitrary crystal orientation. The SLF spectrum was acquired using the pulse sequence of 2D exchange experiment modified by applying FSLG ^{1}H homonuclear decoupling during the t_1 period. The PISEMA spectrum was acquired using the pulse sequence in Fig. 1. In the SLF spectrum, the inclusion of chemical shift makes the dipolar spectra along ω_1 nonsymmetric. A 7-mm MAS probe was operated in the static mode for the measurement. The maximum RF field, $\gamma B_1/2\pi$, was 62 kHz. Other experimental details are described in Fig. 4. A total of 32 t_1 increments were acquired for the 2D PISEMA spectrum with 32 scans for each t_1 increment and a 20-s delay between scans.

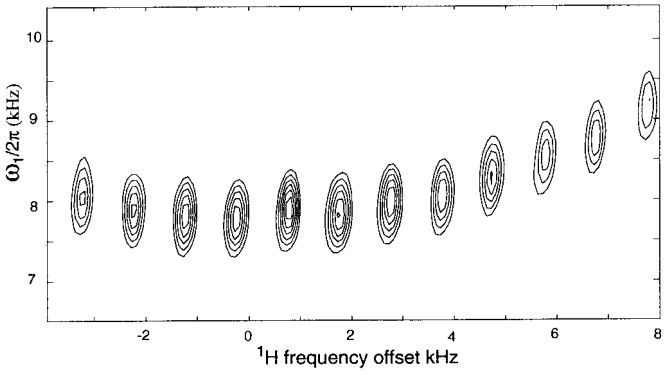

FIG. 6. An array of contour plots of the peak at 112 ppm in Fig. 5b showing the dependence of the PISEMA splitting on the ^{1}H RF frequency.

kHz were recorded (spectra not shown) and it was found that the mismatch has little effect on the dipolar splitting. The proton resonance offset, however, is not averaged by the FSLG sequence and remains effective. Figure 6 shows a peak in the PISEMA spectrum in Fig. 5b with various ^{1}H RF frequencies. The dipolar splitting clearly shows a small quadratic dependence on the ^{1}H resonance offset which is in agreement with the oscillation frequency of spin exchange in Eq. [14], approximated as $D_{S1}\sin\theta_M + (\cos^2\theta_M/2D_{S1}\sin\theta_M)\ \Delta\omega_I^2$. The frequency offset also increases the constant component in the spin exchange and it causes the drop in intensity of the doublet as shown in Fig. 6.

The comparison between the PISEMA and the SLF experiments has been discussed so far only for static samples. The two experiments have been combined with magic angle sample spinning (MAS) for better resolution and sensitivity. Under MAS, the information on dipolar coupling can be extracted from the spinning sideband intensities (*26–28*). In the SLF experiment, the heteronuclear dipolar Hamiltonian mutually commutes at any time during the sample rotation. The broadening from the heteronuclear dipolar coupling is *inhomogeneous*, a term used by Maricq and Waugh, and MAS can effectively narrow the lines even with the spinning rates lower than the heteronuclear coupling (*29*). In the PISEMA experiment, the broadening from the heteronuclear coupling becomes *homogeneous* as the flip-flop dipolar Hamiltonian does not commute as the sample rotates. The difference in line broadening in the SLF and PISEMA spectra of rotating samples is currently under investigation.

4. CONCLUSION

It has been shown that the neighboring protons of a strongly coupled spin pair have little effect on the line broadening in PISEMA spectra. The line narrowing is originated from the truncation of the weak dipolar couplings from neighboring protons by the dominant flip-flop coupling term of the strongly coupled spin pair. This truncation effect is absent in the SLF experiment. In the PISEMA experiment, the mismatch of the Hartmann–Hahn condition is compensated but the ^{1}H resonance offset and the multiple spin effect can distort the dipolar spectra particularly for spin pairs with small dipolar couplings. Despite these effects, the narrow linewidth dramatically increases the resolution of the PISEMA experiment and facilitates the use of heteronuclear dipolar coupling not only for orientational information but also for resolving spectral overlap along the dipolar dimension of the 2D experiment.

ACKNOWLEDGMENTS

The author thanks Prof. D. M. Grant and Dr. D. W. Alderman for kindly providing the methyl-α-D-glucopyranoside single crystal and Prof. T. A. Cross and Dr. R. Fu for helpful discussion. This work is support by the National High Magnetic Field Laboratory through National Science Foundation Cooperative Agreement DMR-9527035 and by the State of Florida.

REFERENCES

1. G. E. Pake, *J. Chem. Phys.* **16,** 327 (1948).
2. J. S. Waugh, *Proc. Natl. Acad. Sci. USA* **73,** 1394 (1976).
3. R. K. Hester, J. L. Ackerman, V. R. Cross, and J. S. Waugh, *Phys. Rev. Lett.* **34,** 993 (1975).
4. S. J. Opella, and J. S. Waugh, *J. Chem. Phys.* **66,** 4919 (1977).
5. L. Muller, A. Kumar, T. Baumann, and R. R. Ernst, *Phys. Rev. Lett.* **32,** 1402 (1974).
6. C. H. Wu, A. Ramamoorthy, and S. J. Opella, *J. Magn. Reson. A* **109,** 270 (1994).
7. M. Lee and W. I. Goldburg, *Phy. Rev. A* **140,** 1261 (1965).
8. A. Bielecki, A. C. Kolbert, H. J. M. deGroot, R. G. Griffin, and M. H. Levitt, *Adv. Magn. Reson.* **14,** 111 (1990).
9. S. J. Opella, F. M. Marassi, J. J. Gesell, A. P. Valente, Y. Kim, M. Oblatt-Montal, and M. M. Montal, *Nat. Struct. Biol.* **6,** 374 (1999).
10. S. J. Opella, *Nat. Struct. Biol./NMR Suppl.* **4,** 845 (1997).
11. F. M. Marassi, A. Ramamoorthy, and S. J. Opella, *Proc. Natl. Acad. Sci. USA* **94,** 8551 (1997).
12. S. R. Hartmann and E. L. Hahn, *Phys. Rev.* **128,** 2042 (1962).
13. A. Pines, M. G. Gibby, and J. S. Waugh, *J. Chem. Phys.* **59,** 569 (1973).
14. R. R. Ernst, G. Bodenhausen, and A. Wokaun, "Principles of Nuclear Magnetic Resonance in One and Two Dimensions" Clarendon, Oxford (1987).
15. P. Jönsson and Å. Kvick, *Acta Crystallogr. B* **28,** 1827 (1972).
16. D. L. VanderHart, H. S. Gutowsky, and T. C. Farrar, *J. Am. Chem. Soc.* **89,** 5056 (1967).
17. A. Naito, S. Ganapathy, and C. A. McDowell, *J. Chem. Phys.* **74,** 5393 (1981).
18. N. Zumbulyadis, P. M. Hendricks, and R. L. Young, *J. Chem. Phys.* **75,** 1603 (1981).
19. J. G. Hexem, M. H. Frey, and S. J. Opella, *J. Chem. Phys.* **77,** 3847 (1982).

20. A. Naito, S. Ganapathy, and C. A. McDowell, *J. Magn. Reson.* **48,** 367 (1982).

21. J. A. DiVerdi and S. J. Opella, *J. Am. Chem. Soc.* **104,** 1761 (1982).

22. J. G. Hexem, M. H. Frey, and S. J. Opella, *J. Am. Chem. Soc.* **105,** 5717 (1983).

23. A. C. Olivieri, L. Frydman, and L. E. Diaz, *J. Magn. Reson.* **75,** 50 (1987).

24. Z. Gan and D. M. Grant, *J. Magn. Reson.* **90,** 522 (1990).

25. R. K. Harris and A. C. Olivieri, *Prog. NMR Spectroscopy* **24,** 435 (1992).

26. J. E. Roberts, G. S. Harbison, M. G. Munowitz, J. Herzfeld, and R. G. Griffin, *J. Am. Chem. Soc.* **109,** 4163 (1987).

27. J. Schaefer, E. O. Stejskal, R. A. McKay, and W. T. Dixon, *J. Magn. Reson.* **57,** 85 (1984).

28. A. J. Ramamoorthy and S. J. Opella, *Solid State Nucl. Magn. Reson.* **4,** 387 (1995).

29. M. M. Maricq and J. S. Waugh, *J. Chem. Phys.* **70,** 3300 (1979).